


System design, analysis, and experimental investigations of linear switched reluctance machines with double mover configuration

Journal of Vibration and Control
2023, Vol. 0(0) 1–13
© The Author(s) 2023
Article reuse guidelines:
sagepub.com/journals-permissions
DOI: 10.1177/10775463231172547
journals.sagepub.com/home/jvc


Aravind CV¹ , Norhisam Misron², Aminath Saadha³, F Azhar⁴,
Albert Alexander Stonier⁵ , and Dishore Shunmugam Vanaja⁶

Abstract

This paper proposes a new double mover configuration of a linear switched reluctance motor (LSRM). The proposed design is established for optimization of the motional forces and to ensure a high-grade electromechanical energy conversion process. The major drawback of the traditional linear machine is that its force densities within and throughout its area is produced in its radial direction of the yoke and does not contribute to its motion or twisting force of the rotor. If these normal forces happen to be in the direction of motion, a larger motional force profile for SRM is yielded. Based on these guidelines, a new LSRM is developed. In order to compare the energy conversion efficiency of LSRM with that of the conventional SRM, a finite element model is constructed. The proposed system is simulated using the FEM software and tested under four conditions. Further, an experimental prototype of the proposed machine is also developed and tested in the laboratory. The results obtained from the prototype indicate that the proposed geometry offers superior performance in terms of high-power density and higher percentage of the national forces.

Keywords

Double mover, high-power density, linear machines, machine design, reluctance motion, teeth optimization

1. Introduction

A linear synchronous motor (LSM) is a linear motor in which the mechanical motion is in synchronism with the magnetic field, that is, the mechanical speed is the same as the speed of traveling magnetic field. In motors with the surface arrangement of magnets, the yoke (back iron) of the reaction rail is ferromagnetic and the permanent magnets (PMs) are magnetized in the normal direction (perpendicular to the active surface) (Kouroussis et al., 2017). The main advantages of these motors are the decreased friction and vibration during starting and running conditions. These types of motors experience fewer energy loss when compared with other motors, since an intermediate gearbox is not necessary for converting rotational motion into linear translation. However, these motors have a limitation. All the existing linear motors utilize PMs for producing the electro-magnetic field required for operation (Abdou and Tereshkovich 2000). In industry, the design of the motor is dependent on the application and has some drawbacks such as complications in average precision and position control, and complications of the control algorithm based on the inductivity of the motor

(Tounsi, 2015). Linear motors are also subjected to the larger air-gaps resulting in lower power densities. For the maximization of the thrust force, stator pole length, air-gap length, winding window width, and stator pole width are considered, which defines the optimization problem

¹Clean Technology Impact Lab, Taylor's University Lakeside Campus, Subang Jaya, Malaysia

²Department of Electrical and Electronic Engineering, Institute of Plantation Studies, Institute of Nanoscience and Nanotechnology, Faculty of Engineering, University Putra Malaysia, Serdang, Malaysia

³Graduate School of Energy Sciences, Kyoto University, Kyoto, Japan

⁴Fakulti Kejuruteraan Elektrik, Universiti Teknikal Malaysia Melaka, Durian Tunggal, Malaysia

⁵School of Electrical Engineering, Vellore Institute of Technology, Vellore, India

⁶Department of Electrical and Electronics Engineering, Mar Baselios College of Engineering and Technology, Thiruvananthapuram, India

Received: 20 September 2022; revised: 28 January 2023; accepted: 5 April 2023

Corresponding author:

Aravind CV, Clean Technology Impact Lab, Taylor's University Lakeside Campus, Subang Jaya, Malaysia.
Email: ChockalingamAravind.Vaithilingam@taylors.edu.my

(Murty et al., 2023). The main objective is to reduce the vibration of the motor while keeping in line with geometrical, thrust, and detent force. As such, several optimization techniques were applied in the design stages such as response surface methodology, genetic algorithm, particle swarm optimization (Wang et al., 2013), and bacterial foraging algorithm (Chittajallu and Lanka 2022) to reduce the vibration of the motor. Linear switched reluctance motor (LSRM) has concentrated windings on the mover which provides the flux flow for translation. These motors are robust with high fault-tolerant capabilities. In specific, these motors do not use the PMs and therefore are easy to manufacture and cheaper. The presence of PM screens in such motors also increases the thrust force and is dependent on the magnetic screen type (Fan et al., 2022). The passive stator topology designed with the power converter is placed in the mover (Xin et al., 2022). This method is cheaper since only one section of the power converter is used; however, it cannot be used in high-speed applications due to the translation of power through the brushes. A new topology for the LSRM with short-pitched and full-pitched winding is presented by Diao et al. (2022). This study focuses on the comparison between the single-sided and double-sided LSRM. The basic model of linear motor used in this work is derived from Prasad et al. (2022). The original LSRM is of a single-sided active stator (SSLRSM). This LSRM has a maximum peak force of 3.05 N with a ripple of 44.85% is the stationary non-moving part and the mover which consists of the coil and is the linear translation component. In the proposed work, the structure of linear reluctance motor has been adapted as a double-sided LSRM (DSL SRM) with single stator and dual mover inbuilt with a coil for the double magnetic circuit. The topologies of these two machines and their magnetic circuits are shown in Figure 1 and Figure 2, respectively. The DSL SRM is formed by the combination of two SSLRSMs as presented is shown in Figure 1. In these machines, the thrust force is doubled and the two sides of the translator balance is the normal force.

Figure 2 shows the equivalent magnetic circuit for both the configurations of the LSRM. As seen from the magnetic circuit, the force of the motor is doubled and the designs of such machines are improved through optimization of the tooth pitch (Gauntt et al., 2022). In this work, the single-sided and double-sided machine is evaluated with a teeth optimization method in which the tooth tapers width is varied for thrust improvement. The LSRM design is derived from the DC linear actuator (Aravind et al., 2013). The tooth width plays an important part in determining the power of the motor as it is proportional to the square of the tooth pitch, “ τ_p .” Zhang et al. (2017) presented the effects of teeth pitch ratio. Petrov et al. (2014) observed that the torque of the system is increased by reducing the saturation through

rearrangement of stator teeth widths. Therefore, it is identified that tooth optimization reduces the armature reaction influence on the produced force. This is supported by the stator comb tooth design modification motor presented by Romlay et al. (2016). Therefore, optimizations in teeth taper are used in this work. The major contributions of the proposed work are as follows:

- The main objective of this paper is to design a new LSRM motor and investigate a new method of controlled electromagnetic system using switched reluctance technology.
- The secondary objective is to use an optimization method through which the vibration of the teeth in the developed system can be reduced to improve the performance of the system.
- The third objective describes about the performance comparison of the existing and developed system.

This paper is organized as follows: Section 2 describes about the design of the suggested system; Section 3 describes about the tooth optimization; Section 4 presents the experimental prototype of the proposed system; Section 5 presents the results of the existing and proposed system. Finally, the proposed work is concluded in Section 6.

2. Proposed system design

The main structure of the linear reluctance motor consists of two parts, namely, the stator, which is the stationary non-moving part and the mover which consists of the coil and is the linear translation component. The structure of a DSL SRM with single stator and dual mover in top view as well as in side view is presented in Figure 3. This assembly includes the LSRM stand, the linear bearing, and the coil case. There are two sections of the LSRM structure, each consisting of 3-phase mover. The 6-phase arrangement allows for various methods of control for the LSRM. The power input to the different phases is controlled through power electronic switches. An excitation circuit can be used to power each phase separately, as shown in Figure 4. The sequential excitation of the phases is carried out through switching the power electronic switches. This makes the LSRM to work in motoring conditions. The sequence of pulse switching for the power electronic switches is presented in Figure 5. The structure can also perform similar operation for a 3-phase system where the U phase and U' phase, V phase, and V' phase, and the W phase and W' phase are interconnected in series and control is processed through power electronic circuits. Advanced commutation methods can also be utilized for increasing the performance of the LSRM.

2.1. Electromagnetic design equations

The work done by the motor is given in equation (1):

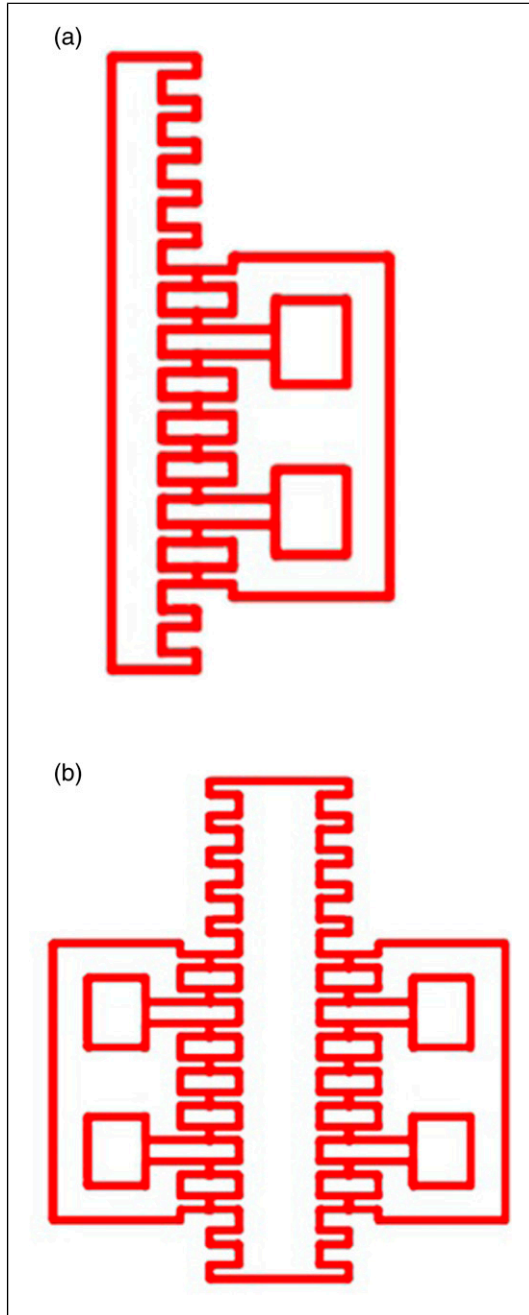


Figure 1. Structure of (a) single-sided SRM and (b) double-sided LSRM.

$$W = p\phi I_z Z \quad (1)$$

where “ I_z ” is the current through the armature conductor, “ Z ” is the total number of armature conductors, “ ϕ ” is the total flux of the pole through which the conductor moves, and “ p ” is the total number of poles. The magnetic loading of the motor is indicated by the right side of the work

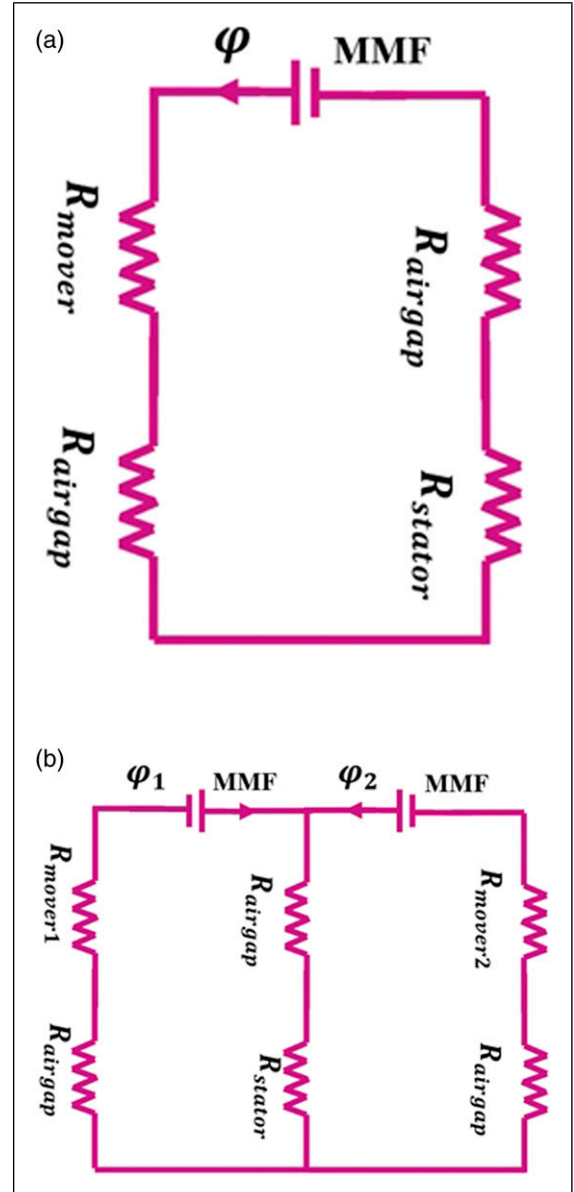


Figure 2. Magnetic circuit of (a) single-sided SRM and (b) double-sided LSRM.

equation and can be used to calculate the specific magnetic loading (B_{av}).

$$B_{av} = \frac{\text{flux per pole}}{\text{area under pole}} \quad (2)$$

$$B_{av} = \frac{\phi}{\tau_p W} \quad (3)$$

where “ τ_p ” is the width of the tooth and “ W ” is the cross-sectional axial length of the motor. Hence, the specific

electrical loading (ac) of the motor is presented in equation (4) and equation (5).

$$ac = \frac{\text{Total armature amp} - \text{conductors}}{\text{Armature periphery at airgap}} \quad (4)$$

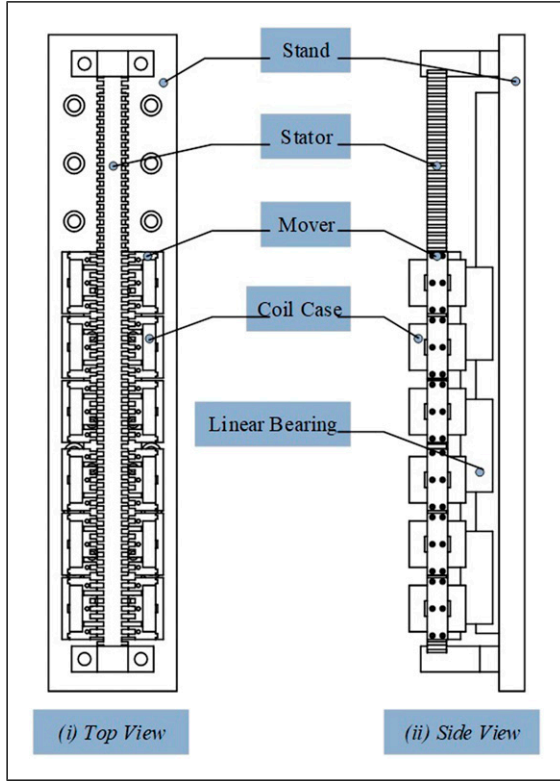


Figure 3. LSRM with double mover configuration.

$$ac = \frac{I_z Z}{L_m} \quad (5)$$

where “ L_m ” is the length of the mover.

The induced electromotive force in the armature is calculated in equation (6).

$$E = \frac{\phi Z \tau_p}{L_m} \quad (6)$$

Therefore, the current through each conductor (I_z) is calculated in equation (7).

$$I_z = \frac{I_a}{a} \quad (7)$$

where “ I_a ” is the total current flowing through the armature and “ a ” is the total number of parallel conductor paths. The power developed in the armature of the motor is thus calculated using equation (9).

$$P_a = EI_a \quad (8)$$

$$P_a = \frac{\phi Z \tau_p}{L_m} \times a I_z \quad (9)$$

By substituting the equations for specific magnetic loading and electrical loading in the equation, we can get the power developed in the armature:

$$P_a = \frac{B_{av} \tau_p W L_m a c \tau_p a}{L_m} \quad (10)$$

$$P_a = \tau_p^2 B_{av} a c W \quad (11)$$

$$P_a = \tau_p^2 W C_0 \quad (12)$$

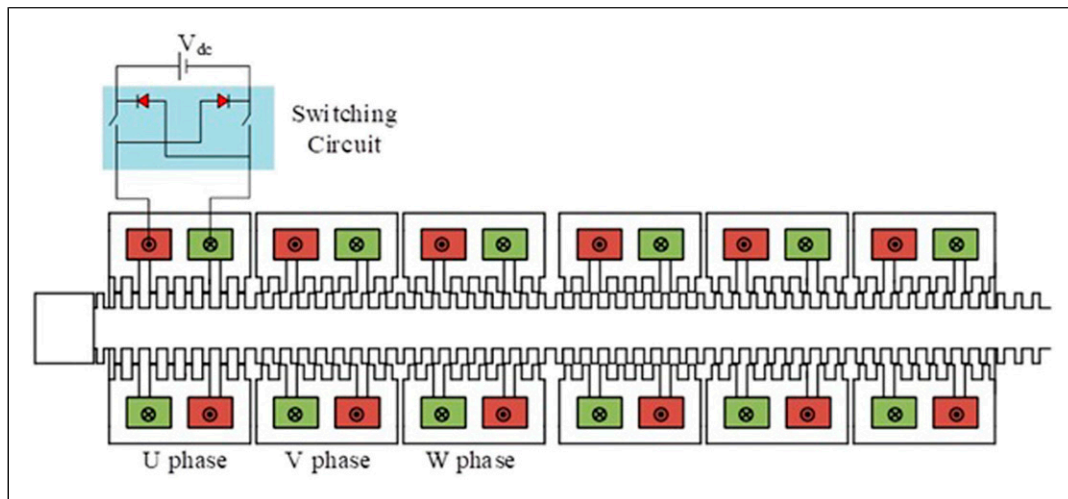


Figure 4. Single phase system with excitation circuit.

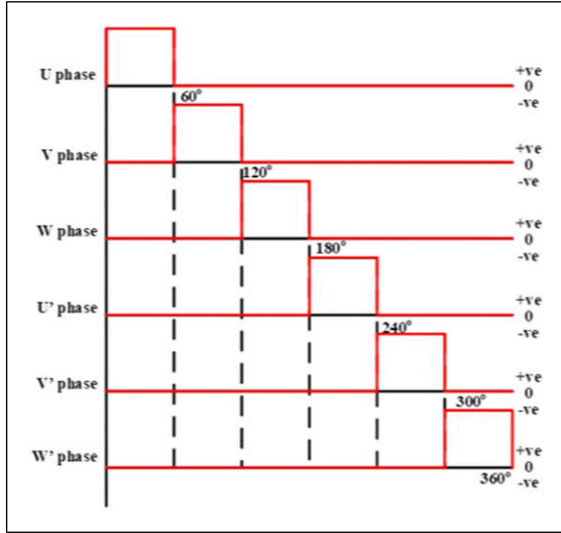


Figure 5. Switching pulses for activating the 6-phases.

$$C_0 = B_{av}ac \quad (13)$$

3. Teeth optimization

One method of removing the vibration of the linear machine is by varying the parameters of teeth width. In this method, the tooth width is kept constant by varying the protruded part T_{ws} , of the teeth, thus finding an optimized ratio for the teeth of both the stator and the mover. Figure 6(a) illustrates the parameters that are to be kept constant and the parameters that have to be changed. Tooth pitch (τ_p) is to be kept constant while varying T_{ws} and as a result of this, variance T_{ss} varies automatically. Two different types of optimizations are conducted and are based on the stator and mover teeth shape modification as shown in Figure 6(b). This is necessary in order to optimize the magnetic flux flowing through the mover's teeth, the air-gap and to the stator teeth, and vice versa. In this work, the tooth pitch τ_p , is changed from 1mm to 6mm, as shown in Figure 6(c). The tooth width T_w , is changed as a function of τ_p , where $T_w = (\text{optimized ratio}) \times \tau_p$. The teeth ratio is kept constant in the suggested work. Simulation work is carried out using the FEM software for four conditions in which the current parameter is changed from 1A, 5A, 7A, and 10A. These values are selected based on the maximum power specification of the motor and is computed based on power loss. Figure 6(d) shows the different aspects of the parameters to be changed in the proposed work. The resolution of angle change is determined by conducting preliminary simulations. In the preliminary simulation, the effect on the thrust of the LSRM at 1A current is observed by changing the angle to 1°. The result of the simulation is indicated in Figure 7. From the results, it is observed that there is not much

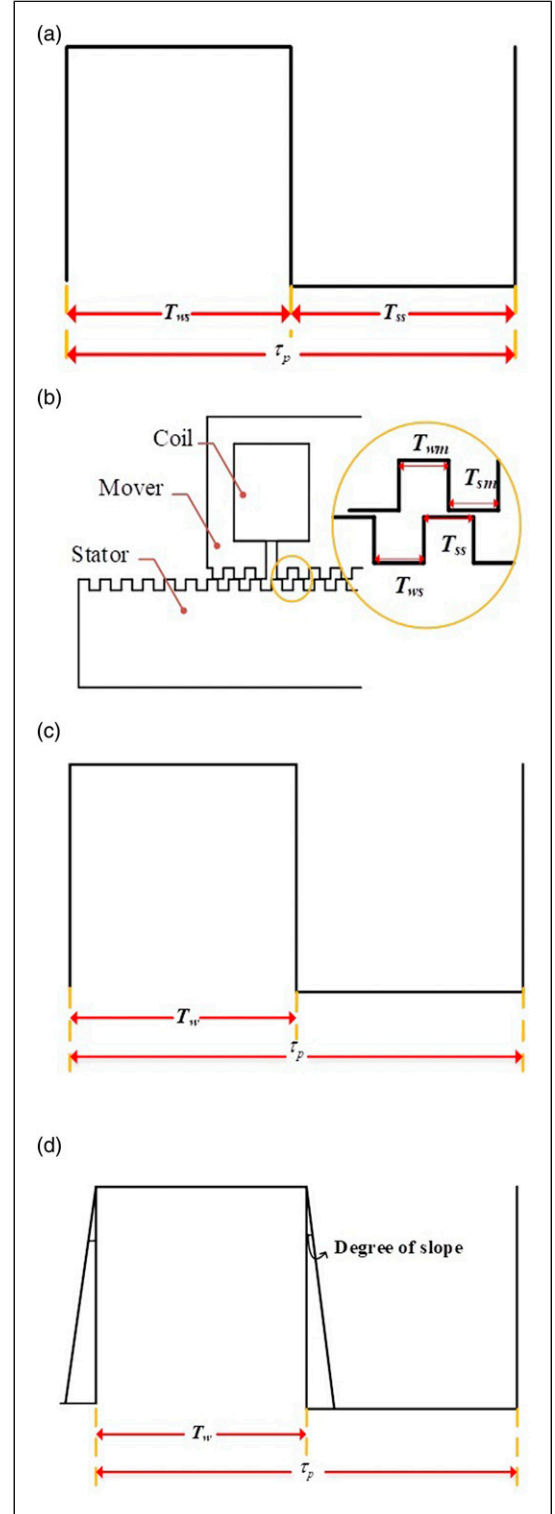


Figure 6. Optimization of teeth.

variation in the thrust force as the angle is increased. There is an average deviation of 0.39% overall when changing from one degree to the next. The highest percentage change is observed at 14°, which is 0.84%. Due to the little

change observed in the thrust force at the low resolution of 1° , it is decided to use a 10-degree resolution in the proposed work. The degrees of angle are then changed to 0° , 10° , and 20° . 20° is the maximum slope angle that can be achieved since the teeth become triangular at that point.

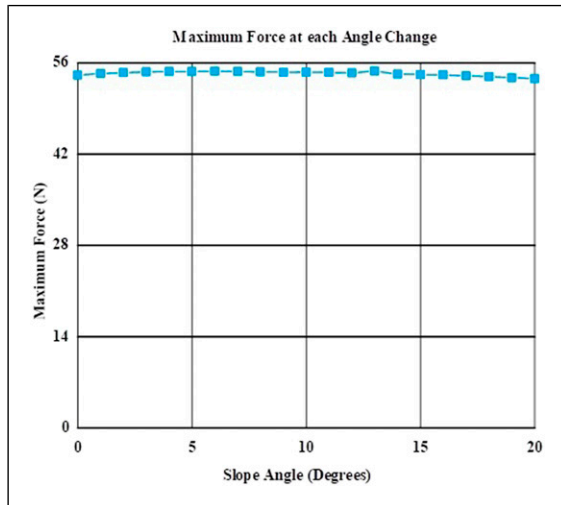


Figure 7. Maximum force developed at each angle change.

4. Experimental design

The prototype of the proposed system is developed from the existing design. The complete assembly is shown in [Figure 8](#). The prototype is of the design dimensions and having a tooth width of 6 mm with an air-gap of 0.5 mm. In the prototype, the air-gap is increased to 0.5 mm for obtaining a uniform air-gap.

The experimental setup comprises of the LSRM, the load cell (which measures the force), the sensor measuring displacement, and the gear arrangement for displacing the mover forward and backward, as shown in [Figure 8](#). Static testing is then conducted on the motor for each phase under different current conditions as mentioned in [Figure 9](#). The LSRM is coupled with the gear arrangement for the forward and backward movement. A constant DC power flows through the coils U and V. The output from the load cell is connected to a converter which then connects to the oscilloscope. The displacement sensor is directly connected to the oscilloscope, which then records both the output values. For each test, the handle is used to provide manual displacement to the mover which then exerts a force on the load cell while moving in the forward and backward direction. These values are then imported into numerical tool for performance analysis.

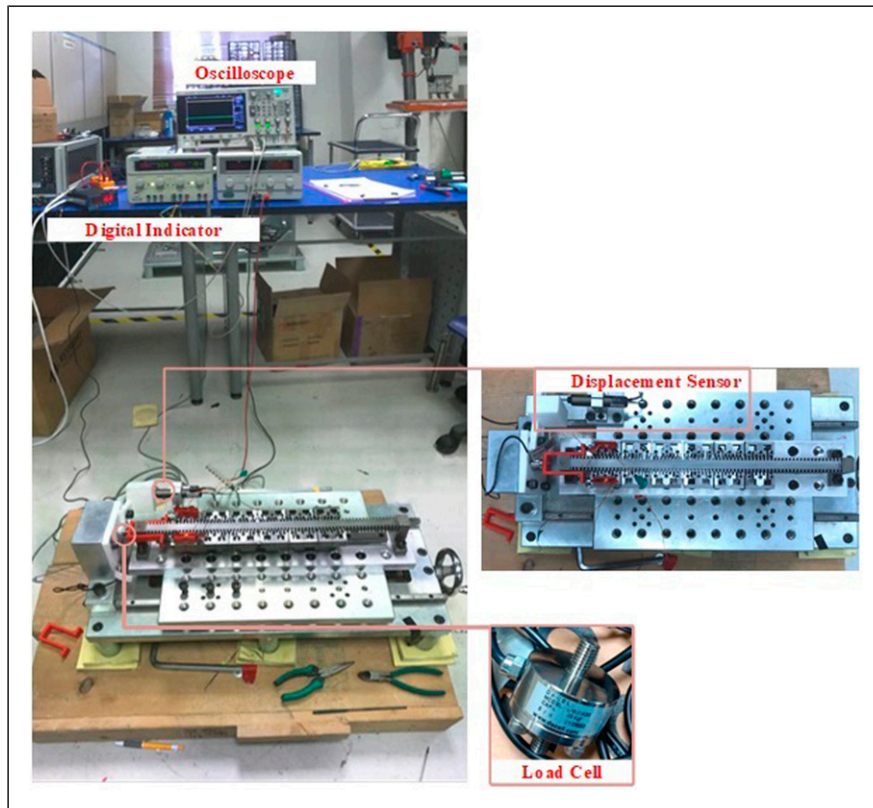


Figure 8. Experimental setup.

5. Results and discussions

5.1. Tooth pitch characteristics

Table 1 shows the changes in the tooth variation for the single-sided and double-sided LSRM. The experimental results are obtained by carrying the test in the prototype. In the prototype, the pitch width $\tau_p = 6.0$ mm is considered with no angle change. During testing, each coil is excited and the force obtained before powering the windings in series are determined. Maximum force is obtained when both the tooth pitch and the current source are increased. It is observed that the force has increased to 63.3% when the pitch width increases from 1 τ_p to 2 τ_p , an increase of 17.8% is observed when the pitch width increases from 2 τ_p to 3 τ_p , an increase of 6.9% is observed when the pitch width increases from 3 τ_p to 4 τ_p , an increase of 0.02% is observed when the pitch width increases from 5 τ_p to 4 τ_p , and finally an increase of 1.44% is obtained when the pitch width increases from 5 τ_p to 6 τ_p at 1A input current. This is because as τ_p increases the amount of space for flux linkage and flux flow increases, thus increasing the flux density and allowing for increased thrust (170N increase at

$\tau_p = 6.0$ mm). The increase in the percentage levels will decrement as the pitch value increases due to saturation of the LSRM. At low current values of 1A, the saturation has already occurred at 4 τ_p . As the current increases, the flux induced by the coil increases, which increases the magnetic field and hence the efficiency and thrust of the machine increases. From Table 1, it is observed that, as the tooth pitch increases the thrust waveform resembles more like a sinusoidal waveform.

The difference in thrust values for the double-sided LSRM is almost twice the increase in thrust value of single-sided LSRM (for $\tau_p = 6$ for single sided, the thrust is at 85 N, while for the double sided, it is at 170 N). This is due to the increase in flux from the double coil and the increased flux linkage from both the sides allowing for an increase in output force. The double-sided configuration allows for the balancing of the normal force, thus allowing for a more sinusoidal waveform. Figure 10 shows the maximum thrust values at each pitch value for different current values of single-sided LSRM. As seen from the graph, the thrust increases with increase in pitch value, and the motor achieves saturation at the pitch value of

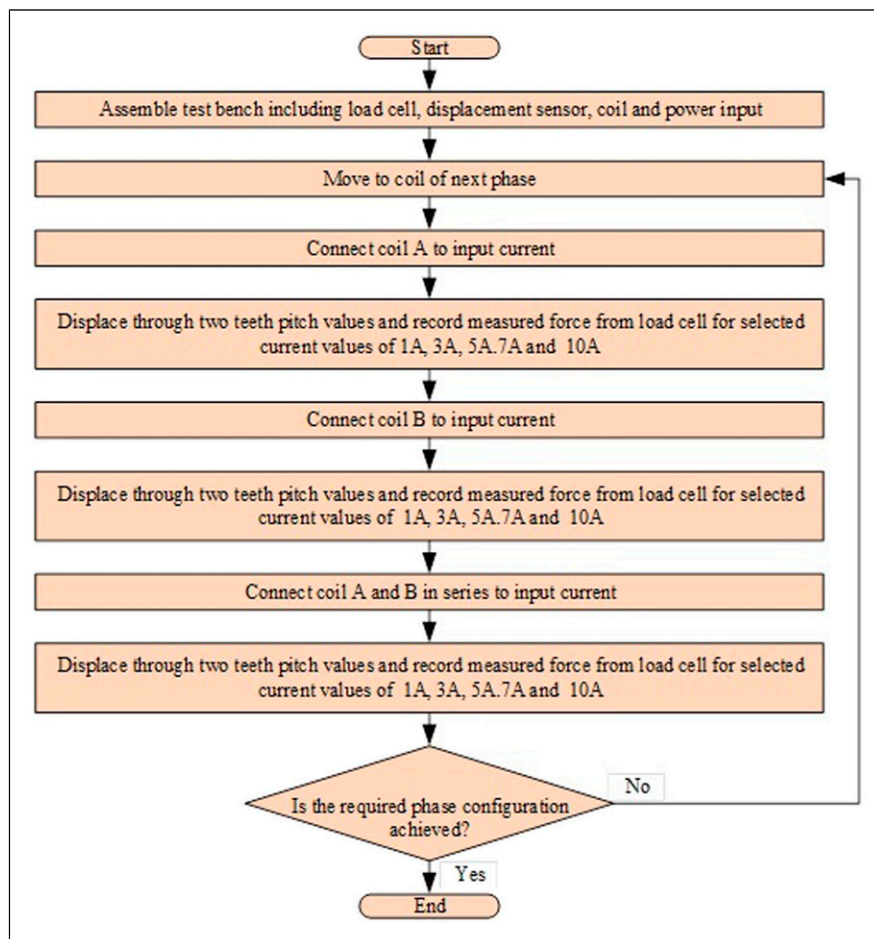
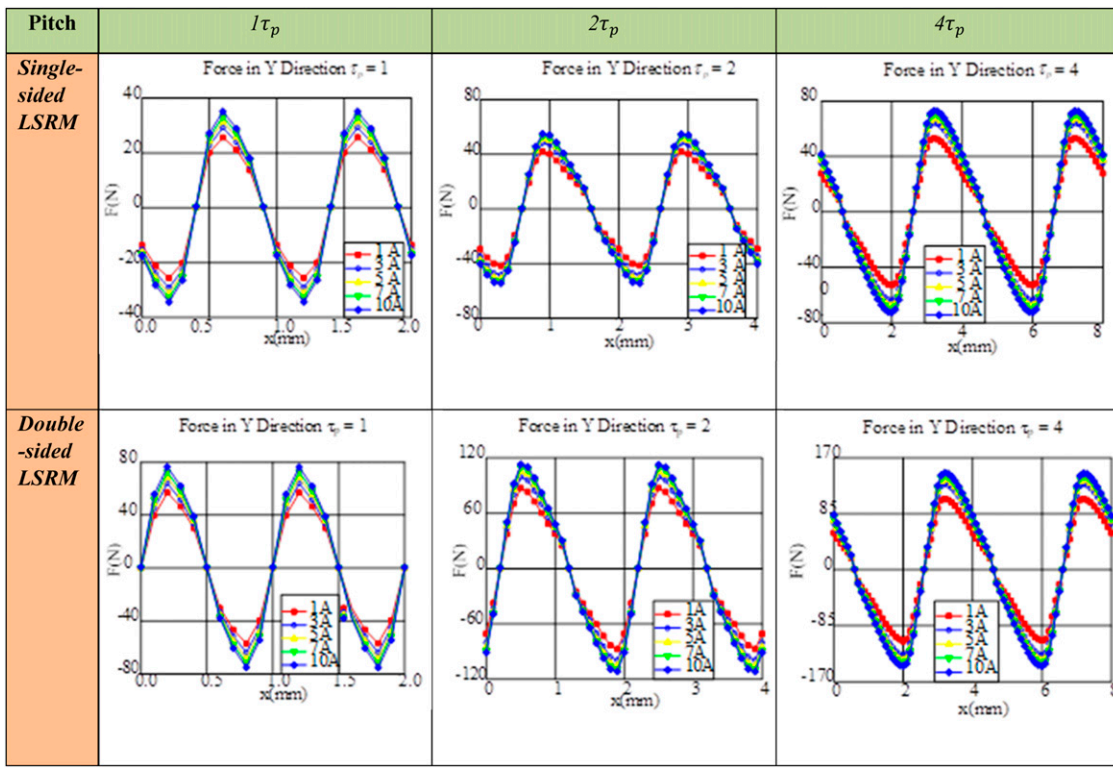


Figure 9. Flowchart of static testing.

Table 1. Tooth pitch variations.



$\tau_p = 6$ mm. The magnetic flux density of the LSRM presented in Figure 11 for $\tau_p = 6$ mm is at 2.04 T. Therefore, at pitch value of $\tau_p = 6$ mm, the LSRM is saturated. Saturation is one of the factors that limit the design of the machine. It governs the maximum allowable flux density and is inherent in the material properties. The material used for the mover and stator in this study is SS400. It is desirable to work these iron parts in higher values of flux density in order to achieve a higher output to weight ratio. The value of the reluctance of the magnetic material is greatly dependent upon the value of flux passing through it. The relative permeability of the ferromagnetic material varies, affecting the saturation levels of the material. The B-H curves of such materials are commonly used for the determination of the excitation value.

5.2. Thrust characteristics

Figure 12 shows the thrust characteristics for the LSRM. From Figure 12, it is observed that the U, V, and W phases are having a phase difference of 120° with each other. This corresponds with the design of the LSRM with a phase difference of 120° . The maximum force that is measured is approximately 4 N observed in Coil A and Coil B at 6A (Table A1 – APPENDIX). As seen from Figure 12, the measured force values are low compared to the simulation data, due to the difference in the air-gap of the prototype which is at 0.5 mm. These low values are

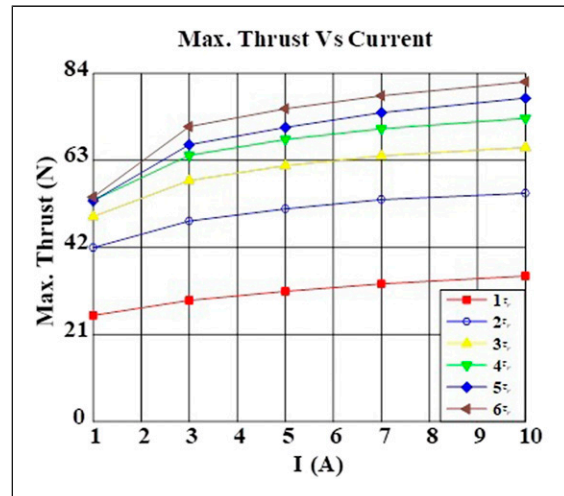


Figure 10. Maximum thrust vs current single-sided LSRM.

obtained due to the differences in air-gap for the manufactured prototype as indicated in Figure 13. Moreover, most phases do not have a constant air-gap and are found to be narrower on one side while wider at the other. This change in the air-gap affects the flux flowing through the mover teeth to the stator teeth and vice versa. The increase in air-gap also increases the reluctance at the point of air-gap.

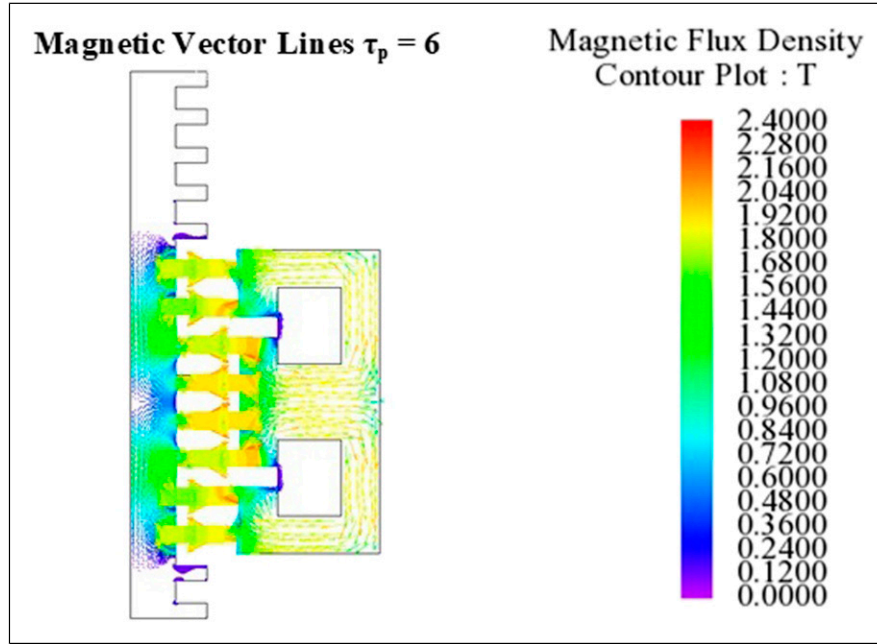


Figure 11. Magnetic flux vector for single sided at $\tau_p = 6$ mm.

Therefore, increasing the chances of flux leakage in the different teeth tips. The translation of the mover during the static experiment also showed that, during displacement, the teeth gap in different areas are also changed constantly and is not kept uniform. These imperfections could make the teeth wider in some places while in others it could be found to be narrower. In addition to this, there may also be changes in the shape of tooth tip, which prevent it from being straight and produces curved edges. Such manufacturing tolerance values can produce non-uniform magnetic strength, density, which in turn fluctuates flux through the teeth, leading to a decrease in the thrust force of the LSRM (Morse et al., 2018; Aravind et al., 2011). These deviations may generate undesired parasitic effects such as torque ripple, losses, or acoustic noise. In order to measure these differences in manufacturing tolerance values, special equipment such as a vision measuring system is required. Due to limitations in obtaining such a machine, this work focuses in the difference in air-gap values which are outlined in the next section.

5.3 Impact of air-gap variations

Experimental investigations are done to understand the effect of a non-uniform or difference in air-gap values to the thrust produced by the LSRM. These investigations are necessary for identifying the manufacturing defects of the LSRM. The manufacturing defects are the difference in air-gap values for the phases, non-uniformity of air-gap at the start and the end of the phase. Therefore, these defects affect the measured force values and decrease the accuracy of the measurement. Figure 14 presents the graphical chart of thrust and airgap.

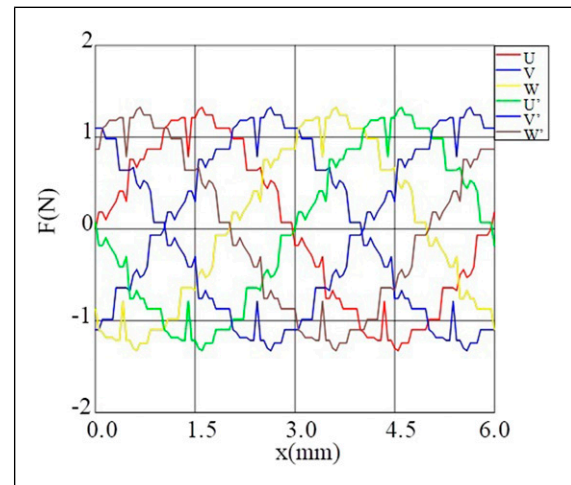


Figure 12. Thrust characteristics for LSRM.

From Figure 14 it is observed that the thrust decreases with increase in the air-gap. It shows an 88.2% decrease from the original simulated value of 0.1 mm air-gap to an air-gap value of 1.5 mm, as shown in Figure 15. This is due to the increase in reluctance with an increase in the length of the gap between the mover and stator causing an increase in leakage flux. Moreover, the flux entering the stator from the air-gap flows into the teeth. There are other losses such as the tooth top leakage flux, where the flux from the mover flows from the top of mover teeth to adjacent mover teeth, instead of flowing to the stator. This leakage flux is increased by the increase in air-gap values.

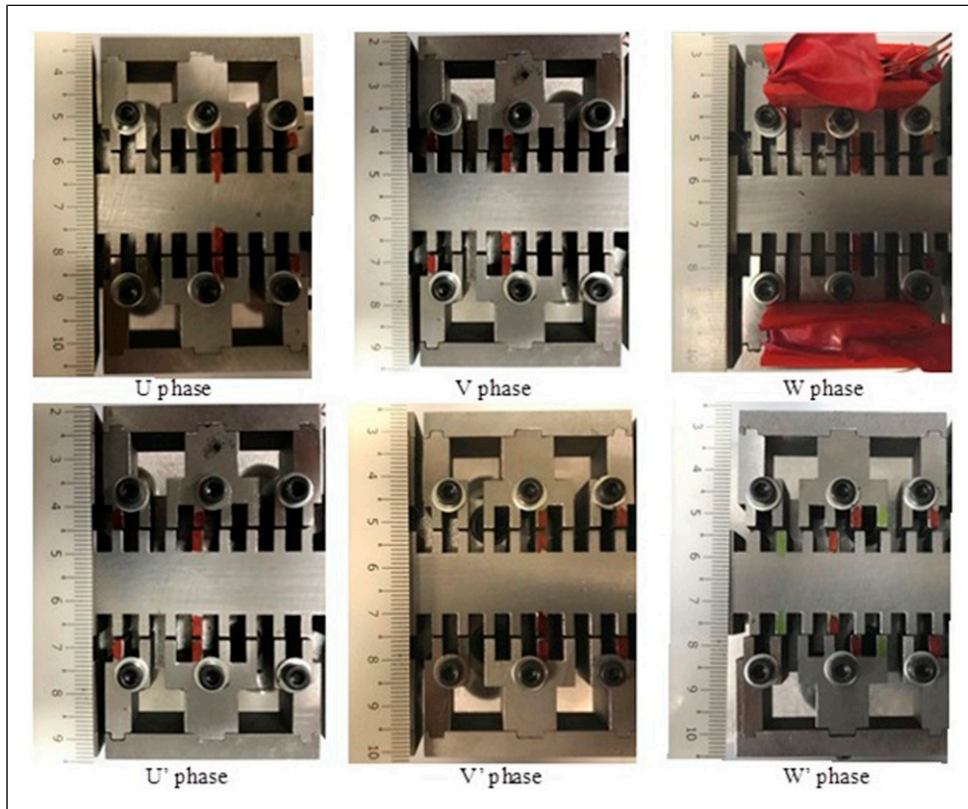


Figure 13. Manufacturing tolerances in the design.

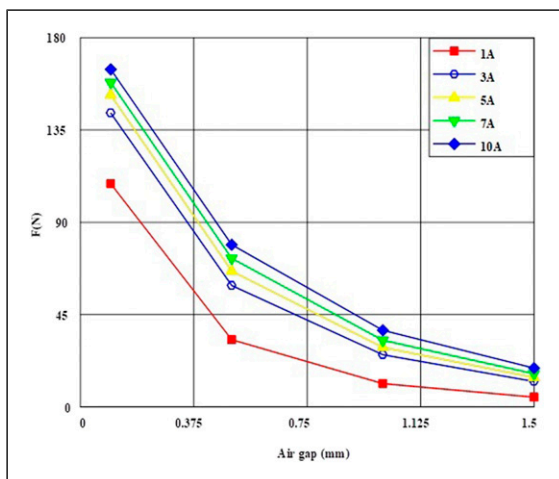


Figure 14. Maximum thrust vs air-gap.

5.4 Comparative evaluations

Table 2 presents the performance evaluation of the un-optimized single-sided and the proposed optimized double-sided motor. For both the experimental and simulation purpose, the motor volume is considered as $5.68 \times 10^{-5} \text{ m}^3$. Since only static testing of the prototype is conducted, the motor constant square density (G) is used as a measure of

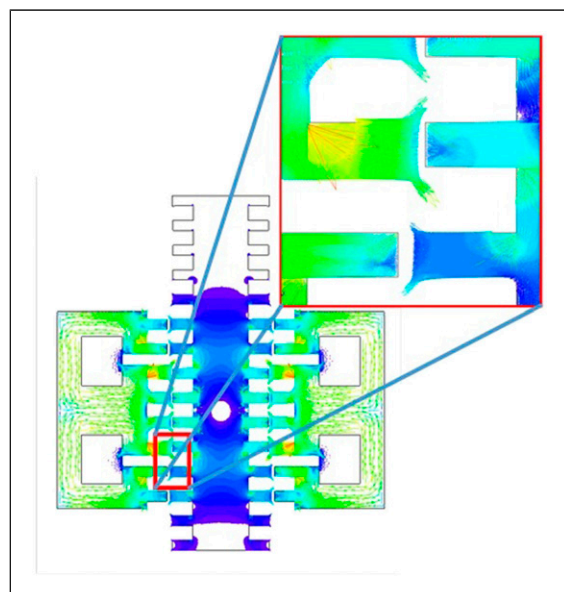


Figure 15. Tooth top leakage flux.

efficiency in the proposed work. From Table 2, it is identified that there is a major variation in the thrust constant, motor constant, and motor constant square density of the conventional and the proposed system. The G value takes

Table 2. Performance parameters of the unoptimized and the optimized motor.

Item	Symbol	FEM	Experimental	Unit
Motor volume	V	5.68×10^{-5}	5.68×10^{-5}	m^3
Thrust constant	K_f	0.866667	0.666667	N/A
Motor constant	K_m	0.732467	0.563436	$N/W^{1/2}$
Motor constant square density	G	9444.232	5588.303	$(N^2/W)/m^3$

Table 3. Comparative evaluation of the proposed system with existing systems.

Item	Symbol	Single-sided LSRM [10]	Modified single-sided LSRM	Proposed double-sided LSRM	Unit
Maximum force	F	40.1	81.9	170.2	N
Motor volume	V	1.08×10^{-4}	2.84×10^{-5}	5.68×10^{-5}	m^3
Thrust constant	K_f	4	8	17	N/A
Motor constant	K_m	1.87	1.75	2.63	$N/W^{1/2}$
Motor constant square density	G	32301.8	108015.5	121939.4	$(N^2/W)/m^3$

into consideration the magnetic force flowing through the motor and the volume of the configuration. As seen from the results of Table 2, it is observed that the motor constant square density G value of the experimental prototype is about 40.82%, while the conventional system has a G value of 28.0%. Therefore, it is found that the proposed DSLSRM design is of high thrust density.

Table 3 presents the comparative analysis of the proposed system with the existing system. From Table 3, it is identified that the G value changes between the unoptimized single-sided LSRM, the optimized single-sided LSRM, and the optimized DSLSRM. The force of the optimized DSLSRM motor is obtained as 170.2 N, whereas as the unoptimized single-sided LSRM and modified single-sided LSRM have about 40.1 N and 81.9 N. This shows that almost the force of the proposed motor has been increased four times when compared with the unoptimized single-sided LSRM and is doubled when compared with the modified single-sided LSRM. Comparing the volume of the three machines, the proposed motor has a volume value of 5.68×10^{-5} which is a lower value when compared with the other two motors thereby giving a higher force to volume ratio. Furthermore, the G value shows an improvement from 32301.8 $(N^2/W)/m^3$ in the unoptimized single-sided LSRM to 121939.4 $(N^2/W)/m^3$ in the optimized double-sided LSRM. This shows that the G value has almost increased to four times when compared with the unoptimized single-sided system. In the single-sided LSRM, the phase windings rotate along with the mover. Due to this arrangement, the single-sided LSRM is more prone to faults and connection issues. In the DSLSRM, the phase windings are separately arranged to avoid the connection issues and failures. In the

single-sided LSRM, a set of linear guides are responsible for keeping the space between the rotor and the stator at a constant distance. Under high current excitations, the force between both the mover and stator teeth can be around 10 times higher than the propulsion force, putting a significant strain on the linear guides and lowering motor performance. The double-sided design utilizes both the magnetic flux and provides symmetry which greatly decreases the normal force. Indirectly the vibration and noise of the machine also gets reduced in this structure, thus improving the performance of the system. Therefore, these results show that the designed LSRM can be utilized as a controlled electromagnetic brake in railway applications.

6. Conclusion

A double-sided LSRM that utilizes a dual magnetic circuit is presented in this paper. The numerical analysis is conducted for the proposed design. The optimized method for the designed prototype model is tested using software FEM calculation and the PAM analysis, respectively. The motor characteristic calculation was done based on motor constant square density (G), and from the results, it is evident that there is a 40.82% and a 28.08% difference between the proposed prototype and the unoptimized LSRM. The experimental analysis presents the results of expected performance indices. Therefore, from the results, it is proved that the double-sided design offers symmetry by employing magnetic flux on both sides. This significantly reduces the normal force. Therefore, the vibration and noise of the machine also gets reduced in this structure, thus improving the performance of the system.

Declaration of conflicting interests

The author(s) declared no potential conflicts of interest with respect to the research, authorship, and/or publication of this article.

Funding

The author(s) disclosed receipt of the following financial support for the research, authorship, and/or publication of this article: This work was supported by the Taylor's Research Grant Scheme TRGS/MFS/1/2016/SOE/005.

Data availability

The required data can be obtained from the corresponding author upon request.

ORCID iDs

Aravind CV  <https://orcid.org/0000-0002-2060-8748>

Albert Alexander Stonier  <https://orcid.org/0000-0002-3572-2885>

References

- Abdou G and Tereshkovich W (2000) Experimental comparison of dynamic FEA results of a permanent magnet brushless DC linear motor. *International Journal of Computer Integrated Manufacturing* 13(3): 214–224.
- Aravind C, Khumira I, Firdaus R, et al. (2013) Single phase flux switching DC linear Actuator. *Journal of Engineering Science and Technology* 1(1): 28–39.
- Aravind CV, Norhisam M, Aris I, et al. (2011). Double-rotor switched reluctance machine (DRSRM): fundamentals and magnetic circuit analysis. In: 2011 IEEE Student Conference on Research and Development, Putrajaya, 19–20 December 2011, pp. 294–299. IEEE.
- Chittajallu T and Lanka RS (2022) An effective controller design for BLDC motor drive with nature inspired heuristic algorithm. In: Proceedings of the International Conference on Artificial Intelligence Techniques for Electrical Engineering Systems (AITEES 2022). Gudlavalluru, 6–7 May 2022, pp. 268–280.
- Diao K, Sun X, Bramerdorfer G, et al. (2022) Design optimization of switched reluctance machines for performance and reliability enhancements: a review. *Renewable and Sustainable Energy Reviews* 168: 112785.
- Fan Z, Liu G, Jin S, et al. (2022) Comparative study on torque characteristics of permanent magnet synchronous reluctance motors with different axial hybrid rotors. *Energy Reports* 8: 1349–1359.
- Gauntt S, McIntyre S and Campbell R (2022) Design optimization of a hybrid spur gear including tooth bending effects. *Journal of the American Helicopter Society* 67(4): 1–15.
- Kouroussis G, Vogiatzis KE and Connolly DP (2017) A combined numerical/experimental prediction method for urban railway vibration. *Soil Dynamics and Earthquake Engineering* 97: 377–386.
- Mohd Romlay FR, Wan Yusoff WA and Mat Piah KA (2016) Increasing the efficiency of traveling wave ultrasonic motor by modifying the stator geometry. *Ultrasonics* 64: 177–185.
- Morse E, Dantan JY, Anwer N, et al. (2018) Tolerancing: managing uncertainty from conceptual design to final product. *CIRP Annals* 67(2): 695–717.
- Petrov I, Ponomarev P and Pyrhönen J (2014) Torque ripple reduction in 12-slot 10-pole fractional slot permanent magnet synchronous motors with non-overlapping windings by implementation of unequal stator teeth widths. In 2014 International Conference on Electrical Machines (ICEM), Berlin, 2–5 September 2014, pp. 1455–1460. IEEE.
- Prasad N, Jain S and Gupta S (2022) Review of linear switched reluctance motor designs for linear propulsion applications. *CES Transactions on Electrical Machines and Systems* 6(2): 179–187.
- Shirish Murty V, Jain S and Ojha A (2023) Linear switched reluctance motor for traction propulsion system using configuration of electric locomotive. *Mechatronics* 89: 102916.
- Tounsi S (2015) Robust design and control of linear actuator dedicated to stamping press application. *International Journal of Electrical Components and Energy Conversion* 1(2): 57–67.
- Wang G, Chen J, Cai T, et al. (2013) Decomposition-based multi-objective differential evolution particle swarm optimization for the design of a tubular permanent magnet linear synchronous motor. *Engineering Optimization* 45(9): 1107–1127.
- Xin Z, Xiong D, Yun T, et al. (2022) Optimal design of linear switched reluctance motor for sea wave power generation. *Global Energy Interconnection* 5(4): 434–447.
- Zhang B, Cheng M, Zhang M, et al. (2017) Comparison of modular linear flux-switching permanent magnet motors with different mover and stator pole pitches. In: 2017 20th International Conference on Electrical Machines and Systems (ICEMS), Sydney, 11–14 August 2017, pp. 1–5. IEEE.

Appendix

Table A1. Measured force value for different currents.

